Noise-aware image deconvolution with multidirectional filters

Hang Yang,[1,*] Ming Zhu,[1] Heyan Huang,[2] and Zhongbo Zhang[2]

[1]Changchun Institute of Optics, Fine Mechanics and Physics, Chinese Academy of Science, Changchun 130033, China

[2]School of Mathematics, Jilin University, Changchun 130012, China

*Corresponding author: yanghang09@mails.jlu.edu.cn

Received 17 July 2013; revised 26 August 2013; accepted 27 August 2013;
posted 27 August 2013 (Doc. ID 194049); published 18 September 2013

In this paper we propose an approach for handling noise in deconvolution algorithm based on multidirectional filters. Most image deconvolution techniques are sensitive to the noise. Even a small amount of noise will degrade the quality of image estimation dramatically. We found that by applying a directional low-pass filter to the blurred image, we can reduce the noise level while preserving the blur information in the orthogonal direction to the filter. So we apply a series of directional filters at different orientations to the blurred image, and a guided filter based edge-preserving image deconvolution is used to estimate an accurate Radon transform of the clear image from each filtered image. Finally, we reconstruct the original image using the inverse Radon transform. We compare our deconvolution algorithm with many competitive deconvolution techniques in terms of the improvement in signal-to-noise ratio and visual quality.

OCIS codes: (100.0100) Image processing; (100.1830) Deconvolution; (100.3190) Inverse problems; (100.3020) Image reconstruction-restoration.

http://dx.doi.org/10.1364/AO.52.006792

1. Introduction

The goal of image deconvolution/deblurring is to reconstruct a true image u_{orig} from a degraded image y that is the convolution of the true image and a point spread function (PSF) h of a linear shift-invariant system $\mathcal{H}$:

$$\begin{aligned} g(n_1,n_2) &= \mathcal{H}u_{\text{orig}}(n_1,n_2)+\gamma(n_1,n_2) \\ &= (h * u_{\text{orig}})(n_1,n_2)+\gamma(n_1,n_2), \end{aligned} \quad (1)$$

where γ is the noise introduced in the procedure of image acquisition, and it is generally assumed to be independent and identically distributed (i.i.d.) zero-mean additive white Gaussian noise (AWGN) with variance σ^2, and "$*$" denotes convolution. The image deconvolution is not only critical to many scientific applications, such as astronomical imaging, remote sensing, camera motion, and medical imaging [1,2], but also important for consumer photography and computational photography [1].

In the discrete Fourier transform domain, Eq. (1) can be written as

$$G(k_1,k_2) = H(k_1,k_2)\cdot U_{\text{orig}}(k_1,k_2)+\Gamma(k_1,k_2), \quad (2)$$

where G, H, U_{orig}, and Γ are the discrete Fourier transform of g, h, u_{orig}, and γ, respectively. Given g and h, we seek to estimate u_{orig}. It is well known that the deconvolution problem is ill-posed. Thus, to obtain a reasonable image estimation, a method of reducing the noise level needs to be utilized.

To find a unique and stable solution, a number of deconvolution algorithms have been proposed. In these methods, the Wiener filter [2,3] and the constrained least squares algorithm [2], can provide a solution to this problem in the frequency domain requiring reduced processing resources. However,

1559-128X/13/276792-07$15.00/0

they often obtain a noisy result with ringing artifacts. As a result, the visual quality of the recovered image often degrades.

Recently, considerable effort has been spent on designing alternative sparsity constraints, which preserve such features. Methods based on these sparsity constraints have been successfully used for image deconvolution. Transformations such as wavelets [4], curvelets [5], shearlets [6], and wave atoms [7] are popular for image representation and are often used for image restoration.

Another popular deconvolution method is based on total variation (TV) [8,9]. The TV deconvolution method finds approximate solutions to differential equations in the space of bounded variation functions. Variations of this method have also been proposed in [10] fast total variation deconvolution, [11] total variation majorization-minimization, [12] total variation shrinkage (TVS). These methods are well known for their edge-preserving properties and generally achieve state-of-the-art results. In [13], iterative shrinkage/thresholding (IST) algorithms were placed on solid mathematical grounds, and fast IST algorithm (FISTA) [14] and two-step IST (TwIST) [15] have improved the IST algorithm.

In particular, the space-variant Gaussian scale mixtures [16], which employs Gaussian scale mixtures in overcomplete directional and multiresolution pyramids, and the block matching 3D [17,18], which employs a nonlocal modeling of images by collecting similar image patches in 3D arrays, are among the current best image deconvolution methods. And it has been shown that learning representation from examples usually achieve good deconvolution results [19,20]. There are many useful algorithms and additional techniques that may be found within [21–26].

In this paper, we propose a new method for estimating a true image from a noisy blurry image. We find that when a directional low-pass linear filter is applied to the blurry image it can reduce the noise level greatly, while the essential blur information along the orthogonal direction is not affected. We then use a deblurring method to estimate the filtered true image and compute its Radon transform along the orthogonal directions of this filter. These projections, known as the Radon transform, will not be affected by the directional filters except for the noise reduction. Based on this observation, we apply a series of directional low-pass filters at different orientations, and estimate a slice of the true image projection from each image. This yields an accurate estimate of the Radon transform. Finally, we reconstruct the true image using the inverse Radon transform. The guided filter-based image deconvolution algorithm, which leads to edge-preserving results, is used in this approach. Through the standard simulation experiments, it outperforms many existing state-of-the-art deconvolution algorithms. Various tests show that our algorithm can perform better than previous approaches on blurry and noisy images.

A. Paper Organization

Section 2 discusses the relationship between multidirection filters and the Radon transform. Then, the general formulation of the proposed deconvolution algorithm is given in Section 3. Next, we demonstrate the effectiveness of our approach by experimenting the new algorithm on several test problems in Section 4. Finally, Section 5 concludes this paper.

2. Multidirectional Filters

We consider the directional low-pass filter l_θ:

$$(I * l_\theta)(n_1, n_2) = \frac{1}{W}\int_{-\infty}^{+\infty} w(t) I(n_1 + t\cos\theta, n_2 + t\sin\theta)\mathrm{d}t, \quad (3)$$

where I is an image, (n_1, n_2) is a pixel location, t is the spatial distance from one pixel to (n_1, n_2), W is the normalization factor defined as $W = \int_{-\infty}^{+\infty} w(t)\mathrm{d}t$. The profile of the filter is determined by $w(t)$, for which we use a Gaussian function, $w(t) = \exp(-t^2/2\sigma^2)$, where σ controls the strength of the filter.

Filtering the blurry image affects the estimated true image. In the filtered image

$$g_\theta = g * l_\theta = h * u * l_\theta + \gamma * l_\theta,$$

we estimate the true image $u_\theta = u * l_\theta$ from g_θ.

Similar to filtering with a two-dimensional (2D) Gaussian filter, the l_θ averages pixels along the direction θ and reduces the noise level. It has nearly no influence on the blur information in the orthogonal direction $\theta + \pi/2$. We exploit this property to estimate the projection of the original image u along the direction θ. The projection can be formulated as a Radon transform [27], which is the collection of integrals of a signal along projection lines. The particular value of the Radon transform corresponding to a projection line $\rho = x\cos\theta + y\sin\theta$ is

$$R_u(\theta, \rho) = \iint u(x, y)\delta(\rho - x\cos\theta - y\sin\theta)\mathrm{d}x\mathrm{d}y, \quad (4)$$

where $u(x, y)$ indicates the value at the coordinate (x, y) on kernel u. θ and ρ are the angle and offset of the projection line, respectively.

Thus, the projection of kernel u_θ along the projection direction θ is

$$R_{u_\theta}\left(\theta + \frac{\pi}{2}, \rho\right) = R_{u * l_\theta}\left(\theta + \frac{\pi}{2}, \rho\right). \quad (5)$$

According to the convolution property of Radon transform

$$R_{f*g}(\theta, \rho) = (R_f(\theta, \cdot) * R_g(\theta, \cdot))(\rho),$$

so Eq. (5) can be written as

$$R_{u_\theta}\left(\theta+\frac{\pi}{2},\rho\right)=\left(R_u\left(\theta+\frac{\pi}{2},\cdot\right)*R_{l_\theta}\left(\theta+\frac{\pi}{2},\cdot\right)\right)(\rho). \tag{6}$$

Note that

$$\begin{aligned}R_{l_\theta}\left(\theta+\frac{\pi}{2},\rho\right)&=\iint l_\theta(x,y)\delta\Big(\rho-x\cos\left(\theta+\frac{\pi}{2}\right)\\&\quad -y\sin\left(\theta+\frac{\pi}{2}\right)\Big)\mathrm{d}x\mathrm{d}y\\&=\frac{1}{W}\int_{-\infty}^{+\infty}w(t)\delta(\rho+t\cos\theta\sin\theta\\&\quad -t\sin\theta\cos\theta)\mathrm{d}t\\&=\delta(\rho).\end{aligned} \tag{7}$$

Then, from Eqs. (6) and (7), we get

$$R_{u_\theta}\left(\theta+\frac{\pi}{2},\rho\right)=R_u\left(\theta+\frac{\pi}{2},\rho\right).$$

It shows l_θ has no impact on the Radon transform of the true uncorrupted image to the orthogonal direction of the filter. This is the foundation of the proposed approach. An example is shown in Fig. 1.

3. Deconvolution Algorithm

A. Noise-aware Image Estimation

Based on the analysis above, we apply a directional filter l_θ, estimate the filtered true image u_θ, and then project it along the orthogonal direction of the filter to get the corresponding Radon transform. We repeat this process to get a set of projections. Finally, we compute the 2D image using the inverse Radon transform [27]. The advantage of this strategy is that it greatly reduces noise when applying l_θ, while keeping the computed Radon transform intact.

We summarize the proposed algorithm as follows, Steps 1 to 4 are also illustrated in Fig. 2.

Algorithm 1 Noise-aware Image Deconvolution Algorithm

Input: Blurry and noisy image g and PSF h.

Output: Estimated image u.

1. Apply N_d directional smoothing filters to the input image g, each filter has a direction of $k\pi/N_d$, $k=1,\ldots,N_d$, where N_d is the number of directional filters.
2. For each filtered image g_θ, use PSF h to estimate u_θ.
3. For each estimated u_θ, compute its Radon transform $R_{u_\theta}(\theta+(\pi/2),\rho)$ along the direction $\theta+(\pi/2)$.
4. Reconstruct u from the series of $R_{u_\theta}(\theta+(\pi/2),\rho)$ using inverse Radon transform.

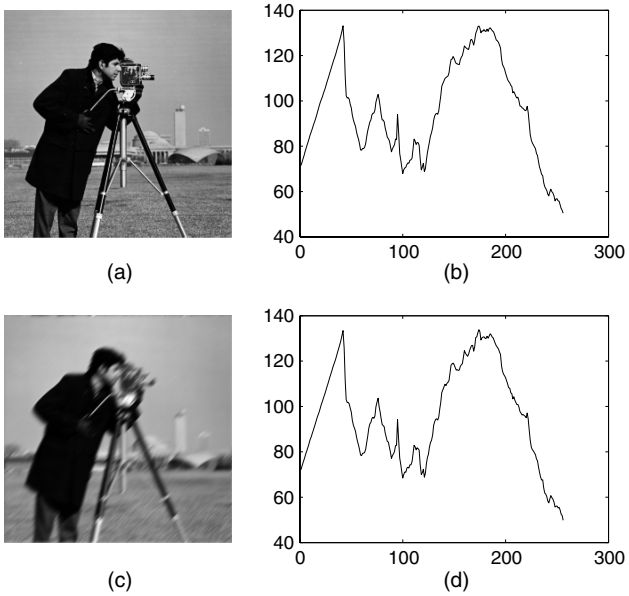

Fig. 1. Directional filter and the Radon transform. (a) Original image, (b) Radon transform of original image along the $\theta=3\pi/4$, (c) filtered image by apply the directional filter ($\theta=\pi/4$), and (d) Radon transform of filtered image along the $\theta=3\pi/4$. Note that the Radon transform of the filtered image is the same as the original unfiltered image.

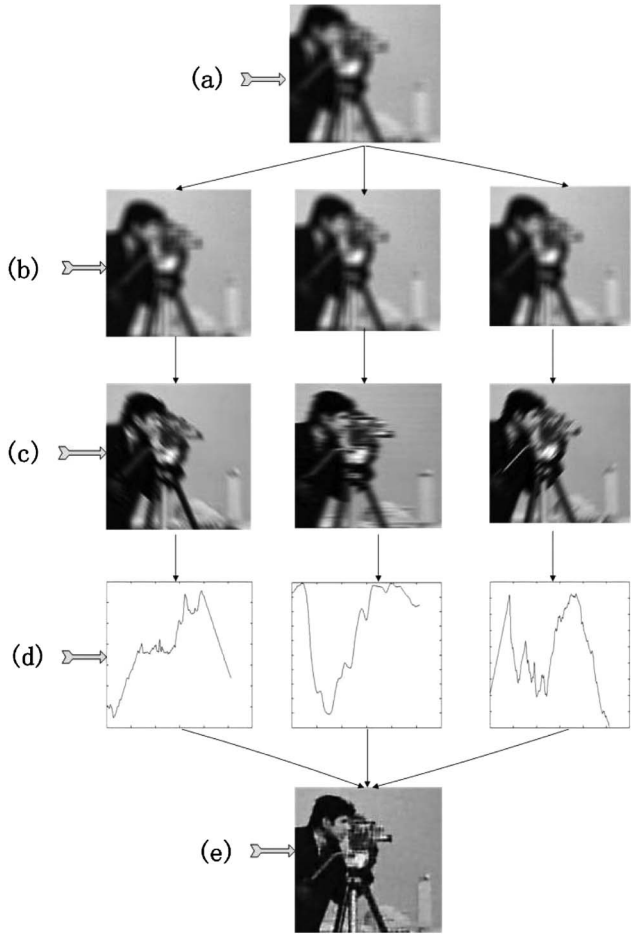

Fig. 2. Illustration of applying directional filters for image deblurring. (a) Blurred noisy image. (b) We apply directional filters in different orientations to the blurred noisy image. (c) From each filtered image, a deblurred image is computed first, then (d) projected along the orthogonal direction to generate the correct Radon transform of the true image. (e) Final true image u is reconstructed using inverse Radon transform.

In Step 2, since noise is largely removed by the directional filtering, we apply a robust deconvolution technique described in Section 3.B to estimate the filtered image u_θ. This novel technique is based on guided filters [28]. In [26], we first integrate the guided filter into the deconvolution problem to propose an efficient iterative algorithm, which leads to high-quality reconstruction results. In this work, we improve the method proposed in [26] to adapt the directional filtered images.

B. Guided Filter-Based Image Deconvolution

Image smooth with guided filter was defined in [28]. To date, it is one of the fastest edge-preserving filters. The key assumption of the guided filter is a local linear model between the guidance image and the filtering output image. The guided filter output is locally a linear transform of the guidance image. This filter has the edge-preserving smoothing property like the bilateral filter, but does not suffer from the gradient reversal artifacts. So we integrated this filter into the deconvolution problem.

In our approach, we minimize the following energy function to estimate every filtered image u_θ:

$$\min_{u_\theta}\|g_\theta - h * u_\theta\|^2 + \lambda\|u_\theta - \mathtt{Guid}(p_\theta, u_\theta)\|^2, \quad (8)$$

where $\mathtt{Guid}(\cdot)$ is the guided filter smoothing operation [28], λ is a balancing weight, and p_θ is the guidance image.

Minimizing this energy function will ensure that the deblurred image is noise artifact free, and can best fit u_θ and g_θ. Directly minimizing this energy is hard because $\mathtt{Guid}(\cdot)$ is highly nonlinear. Our algorithm is based on the decouple of deblurring and denoising steps in the restoration process.

In the deblurring step, we proposed two cost functions:

$$u_\theta = \arg\min_{u_\theta}\|g_\theta - h * u_\theta\|^2 + \lambda\|u_\theta - \bar{u}_\theta\|^2, \quad (9)$$

$$p_\theta = \arg\min_{p_\theta}\|g_\theta - h * p_\theta\|^2 + \lambda\|\nabla_\theta p_\theta - \nabla_\theta \bar{u}_\theta\|^2, \quad (10)$$

where $\bar{u}_\theta$ is a pre-estimated image. For initialization we set $\bar{u}_\theta$ to be zero (a black image).

To suppress the amplified noise and artifacts introduced by Eq. (9) in the denoising step, we applied the guided filter to smooth the estimated image u_θ, and p_θ is used as the guidance image:

$$\bar{u}_\theta = \mathtt{Guid}(p_\theta, u_\theta). \quad (11)$$

The image u_θ contains more noise and image information than p_θ. So we use p_θ as the guidance image and u_θ as the filtering input image to recover some details and reduce the leaked noise.

Different from [26], we use the directional gradient operator ∇_θ instead of the gradient operator ∇ in Eq. (11), where $\nabla_\theta = \nabla \times R_\theta = (\partial_x, \partial_y) \times R_\theta$ is the directional gradient operator, $R_\theta = \left(\begin{smallmatrix}\cos\theta & \sin\theta \\ -\sin\theta & \cos\theta\end{smallmatrix}\right)$. Since l_θ filters along the direction θ, they have an influence on the profile of edges. We use the directional derivative operator along the θ and $\theta + \pi/2$ instead of gradient operator (along 0 and $\pi/2$), to suit for the change of image's edges.

Alternatively, we diagonalized derivative operators after the fast Fourier transform (FFT) has been applied to reduce the computational complexity. These yield solutions of Eqs. (10) and (11) in the Fourier domain

$$\mathcal{F}(u_\theta) = \frac{\mathcal{F}(h)^* \cdot \mathcal{F}(g_\theta) + \lambda\mathcal{F}(\bar{u}_\theta)}{|\mathcal{F}(h)|^2 + \lambda}, \quad (12)$$

$$\mathcal{F}(p_\theta) = \frac{\mathcal{F}(h)^* \cdot \mathcal{F}(g_\theta) + \lambda|\mathcal{F}(\nabla_\theta)|^2 \cdot \mathcal{F}(\bar{u}_\theta)}{|\mathcal{F}(h)|^2 + \lambda|\mathcal{F}(\nabla_\theta)|^2}, \quad (13)$$

where $\mathcal{F}$ is the FFT operator, $\mathcal{F}(\cdot)^*$ denotes the complex conjugate, and

$$\begin{aligned}|\mathcal{F}(\nabla_\theta)|^2 &= |(\mathcal{F}(\partial_x), \mathcal{F}(\partial_y)) \times R_\theta|^2 \\ &= |\mathcal{F}(\partial_x)\cos\theta - \mathcal{F}(\partial_y)\sin\theta|^2 \\ &\quad + |\mathcal{F}(\partial_x)\sin\theta + \mathcal{F}(\partial_y)\cos\theta|^2,\end{aligned}$$

denotes the Fourier transform of ∇_θ operator. The plus, multiplication, and division are all componentwise operators.

We found that iterating Eqs. (9)–(11) yields a good result in practice. Solving Eq. (9) yields a noisy image u_θ that also contains useful high-frequency image structures. In the alternating minimization process, the noise in u_θ is gradually reduced, while the high-frequency image details are preserved by guided image filter. So, this leads to an algorithm that produces high quality image reconstructions.

4. Experiments

In this section, we present results of our proposed algorithm and compare it against competing deblurring methods such as ForWaRD [4], TVS [12], L0-AbS [22], SURE-LET [25].

In these experiments we will use the improvement in signal-to-noise ratio (ISNR) to measure the performance. The ISNR is defined as

$$\mathrm{ISNR} = 10\log_{10}\left(\frac{\|u_{\mathrm{orig}} - g\|_2^2}{\|u_{\mathrm{orig}} - \hat{u}\|_2^2}\right),$$

where $\hat{u}$ is the corresponding estimated image.

For all the experiments, we set the extent σ of the directional filter to 15 pixels. If the size of the image is $N \times N$, we apply directional filters along N regularly sampled orientations. In our work [26], a simple but effective method was proposed for determining the parameter of Eq. (8) automatically.

We consider six benchmark deconvolution problems. In these experiments, original images are *Cameraman* (experiments 1, 2, and 3) of size

Table 1. Description of the Observation Parameters for the Six Experiments

	Blur	σ^2
Exp. 1	9×9 *uniform*	4
Exp. 2	$h_{i,j} = (1 + i^2 + j^2)$, $i, j = -7, \ldots, 7$	16
Exp. 3	25×25 Gaussian PSF with standard deviation 1.6	8
Exp. 4	$[1, 4, 6, 4, 1]^T [1, 4, 6, 4, 1]/256$	64
Exp. 5	25×25 Gaussian PSF with standard deviation 1.6	8
Exp. 6	9×9 *uniform*	4

256×256, *Lena* of size 512×512 (experiment 4), *House* of size 256×256 (experiment 5) and *Boat* of size 512×512 (experiment 6). Table 1 summarizes the different degradation models used, which are defined by the blur type and the variance of the AWGN for each of the experiments. The original images are shown in Fig. 3. We have tested our method with different blur models at various noise levels. Good and consistent results have been achieved.

In the experiments, the proposed method outperforms the other techniques in terms of ISNR. We note that the results of the six standard experiments for different images are included in Table 2 as follows.

In the first set of experiments, a *Cameraman* image, shown in Fig. 4(a), is blurred by a 9×9 uniform box-car blur. The AWGN variance is $\sigma^2 = 4$. The ISNR values obtained by the different methods are compared in Table 2 under experiment 1 column. The proposed method yields ISNR values of 6.16 dB, which are better than the values obtained by any of the other methods. A portion of the image

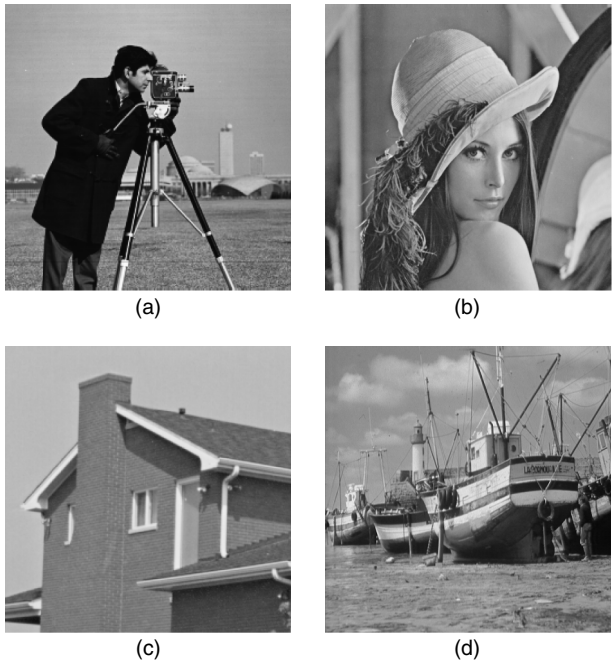

Fig. 3. Images used in this paper for different experiments. (a) Cameraman image, (b) Lena image, (c) house image, and (d) boat image.

Table 2. ISNR for Different Experiments

Methods	Exp. 1	Exp. 2	Exp. 3	Exp. 4	Exp. 5	Exp. 6
Our method	6.16	5.18	3.40	5.01	4.99	5.61
ForWaRD	4.88	4.31	2.83	3.21	3.53	4.75
TVS	5.72	4.52	3.11	4.12	4.51	5.20
L0-AbS	5.45	4.37	3.02	4.42	4.55	5.25
SURE-LET	5.08	4.21	2.95	4.80	4.02	5.41

is zoomed to reveal the visual detail of the results obtained by the different methods, and is shown in Figs. 4(a)–4(f). As can be seen from Fig. 4(c), the result of ForWaRD method [4] obtains a low-contrast image with some visual artifacts. The results of TVS [12] and L0-Abs [22] are shown in Figs. 4(d) and 4(e), respectively. It can be seen that some details on the man's face are lost. The restoration result of our proposed method is shown in Fig. 4(f). It is noticeable that our result preserves the edge better (see, the man's face), and recovers more image details than the competing methods.

In the second set of experiments (Exp. 2 and Exp. 3) performed over the *Cameraman* image, the blur kernel (PSF) and the noise variances are shown in Table 1. The simulation results are reported under Exp. 2 and Exp. 3 of Table 2, respectively. As can be seen from the ISNR, our algorithm shows the best performance compared to other image deconvolution methods.

In the third set of tests, a *Lena* image, shown in Fig. 3(b), is blurred by a 5×5 separable filter with weights $[1, 4, 6, 4, 1]/16$ in both the horizontal and vertical directions and then contaminated with AWGN by $\sigma = 8$. The results are summarized under Exp. 4 column of Table 2. A portion of the deblurred images from different methods are shown in Fig. 5. In Figs. 5(c)–5(f), it can be seen that there are no slight differences among them in the visual performance. The reason for this may be that the size of

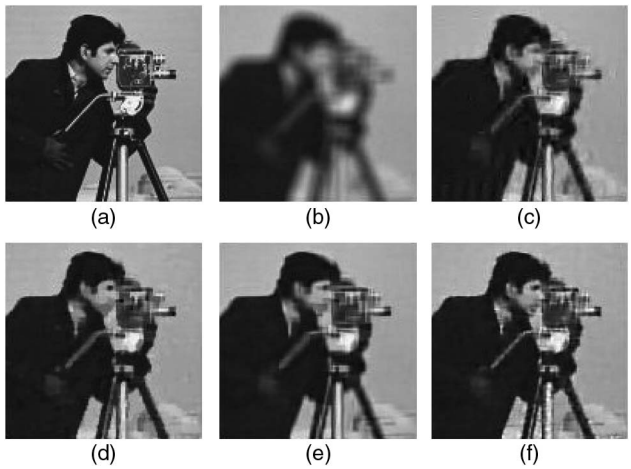

Fig. 4. Details of the image deconvolution experiment with a *Cameraman* image. (a) Original image, (b) blurred image, (c) ForWaRD result, ISNR = 4.88 dB, (d) TVS result, ISNR = 5.72 dB, (e) L0-AbS result, ISNR = 5.45 dB, and (f) our result, ISNR = 6.16 dB.

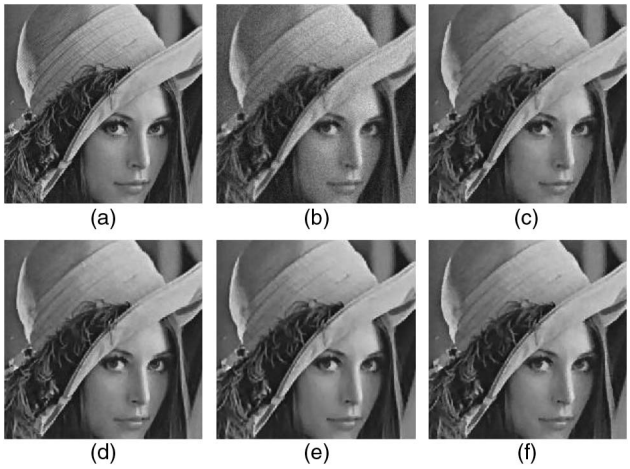

Fig. 5. Details of the image deconvolution experiment with a *Lena* image. (a) Original image, (b) blurred image, (c) TVS result, ISNR = 4.12 dB, (d) L0-AbS result, ISNR = 4.42 dB, (e) SURE-LET result, ISNR = 4.80 dB, and (f) our result, ISNR = 5.01 dB.

the PSF is small (5 × 5), the blur effect of degraded image [shown in Fig. 5(b)] is not obvious. But our multidirectional filters algorithm performs the best in terms of ISNR. This experiment shows that even in the case of extreme noise levels, our method can provide better reconstruction than some of the competitive deconvolution methods.

In the fifth experiment, we apply a Gaussian PSF on the *House* image. The deconvolution results obtained by different methods are reported under Exp. 5 column of Table 2. Our multidirectional filter based method performed, yielding ISNR values of 4.99 dB. The details of the images obtained by the different methods are shown in Fig. 6. The result of TVS [12] is shown in Fig. 6(c), there are some blocking artifacts in the image. The restoration result of the L0-AbS algorithm [22] is shown in Fig. 6(d), it can bee seen that the vertical white edge

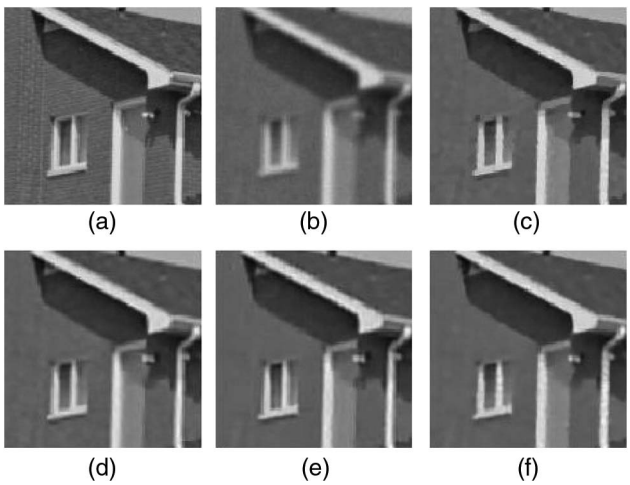

Fig. 6. Details of the image deconvolution experiment with a *House* image. (a) Original image, (b) blurred image, (c) TVS result, ISNR = 4.51 dB, (d) L0-AbS result, ISNR = 4.55 dB, (e) SURE-LET result, ISNR = 4.02 dB, and (f) Our result, ISNR = 4.99 dB.

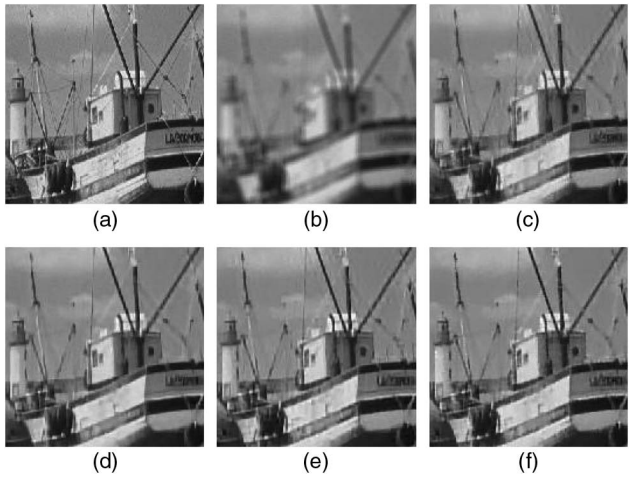

Fig. 7. Visual comparison of *Boat* image in Exp. 6. (a) Crop from *Boat* image, (b) blurred image, (c) ForWaRD result, ISNR = 4.75 dB, (d) L0-AbS result, ISNR = 5.25 dB, (e) SURE-LET result, ISNR = 5.41 dB, and (f) our result, ISNR = 5.61 dB.

of the wall is still blurry. Figure 6(e) shows the result of SURE-LET [25]. By careful examination, we see that there are a few artifacts around the vertical edges in window. Our result is shown in Fig. 6(f). It is obvious that our method recovers the sharpness of some edges (for instance, vertical edges in window). This experiment shows that our proposed method can provide better reconstruction than some of the competing deconvolution methods.

In the final experiment, the original image of *Boat* is blurred by a 9 × 9 uniform box-car blur, the noise variances are $\sigma^2 = 4$. From Table 2, we notice that our method performs the best in terms of ISNR. The restoration result of the ForWaRD [4] is shown in Fig. 7(c). By careful examination we find that there are some visually annoying artifacts in the image. The restoration result of the L0-AbS algorithm [22] is shown in Fig. 7(d). It can be seen that some image details on the boat are lost. The restoration result of SURE-LET [25] is shown in Fig. 7(e), there are a few artifacts around the side of boat. The restoration result of our proposed method is shown in Fig. 7(f). One can see that it is more visually pleasant than Figs. 7(c)–7(e). Results have shown that the multidirectional filters-based method obtains a deblurring result with better quantitative and visual performance.

5. Conclusion and Future Work

In this paper, we presented a deconvolution method based on multidirectional noise removal filters using a Radon transform. We use directional filters to reduce the effect of the noise while keeping the image information unaffected in its orthogonal direction. By applying a series of directional filters, we showed how to recover correct one-dimensional projections of the true image in all directions, which we use to estimate an accurate image using the inverse Radon transform. We also introduced a noise-tolerant nonblind deconvolution technique based on guided

filters, which leads to high-quality reconstruction results. The proposed method was tested using synthetic experiments and outperformed four existing state-of-the-art deconvolution algorithms. The proposed model and algorithm can be extended to more general image restoration problems such as denoising and super-resolution.

References

1. A. K. Jain, *Fundamental of Digital Image Processing* (Prentice-Hall, 1989), pp. 267–341.
2. A. K. Katsaggelos, ed., *Digital Image Restoration* (Springer, 1991), pp. 24–41.
3. P. C. Hansen, *Rank-Deficient and Discrete Ill-Posed Problems: Numerical Aspects of Linear Inversion* (SIAM, 1998).
4. R. Neelamani, H. Choi, and R. G. Baraniuk, "ForWaRD: Fourier-wavelet regularized deconvolution for ill-conditioned systems," IEEE Trans. Signal Process. **52**, 418–433 (2004).
5. J. Starck, M. K. Nguyen, and F. Murtagh, "Wavelets and curvelets for image deconvolution: a combined approach," Signal Process. **83**, 2279–2283 (2003).
6. V. M. Patel, G. R. Easley, and D. M. Healy, Jr., "Shearlet-based deconvolution," IEEE Trans. Image Process. **18**, 2673–2685 (2009).
7. H. Yang and Z. Zhang, "Fusion of wave atom-based wiener shrinkage filter and joint non-local means filter for texture-preserving image deconvolution" Opt. Eng. **51**, 067009 (2012).
8. L. Rudin, S. Osher, and E. Fatemi, "Nonlinear total variation based noise removal algorithms," Physica D **60**, 259–268 (1992).
9. T. Chan, S. Esedoglu, F. Park, and A. Yip, "Recent developments in total variation image restoration," *Handbook of Mathematical Models in Computer Vision* (Springer, 2005).
10. Y. Wang, J. Yang, W. Yin, and Y. Zhang, "A new alternating minimization algorithm for total variation image reconstruction," SIAM J. Imag. Sci. **1**, 248–272 (2008).
11. J. Oliveira, J. M. Bioucas-Dias, and M. A. Figueiredo, "Adaptive total variation image deblurring: a majorization-minimization approach," Signal Process. **89**, 1683–1693 (2009).
12. O. V. Michailovich, "An iterative shrinkage approach to total-variation image restoration," IEEE Trans. Image Process. **20**, 1281–1299 (2011).
13. I. Daubechies, M. Defrise, and C. De Mol, "An iterative thresholding algorithm for linear inverse problems with a sparsity constraint," Commun. Pure Appl. Math. **57**, 1413–1457 (2004).
14. A. Beck and M. Teboulle, "A fast iterative shrinkage-thresholding algorithm for linear inverse problems," SIAM J. Imag. Sci. **2**, 183–202 (2009).
15. J. Bioucas-Dias and M. Figueiredo, "A new TwIST: two-step iterative shrinkage/thresholding algorithms for image restoration," IEEE Trans. Image Process. **16**, 2992–3004 (2007).
16. J. A. Guerrero-Colon, L. Mancera, and J. Portilla, "Image restoration using space-variant Gaussian scale mixtures in overcomplete pyramids," IEEE Trans. Image Process. **17**, 27–41 (2008).
17. K. Dabov, A. Foi, V. Katkovnik, and K. Egiazarian, "Image denoising by sparse 3D transform-domain collaborative filtering," IEEE Trans. Image Process. **16**, 2080–2095 (2007).
18. K. Dabove, A. Foi, V. Katkovnik, and K. Egiazarian, "Image restoration by sparse 3D transform-domain collaborative filtering," Proc. SPIE **6812**, 681207 (2008).
19. J. Mairal, M. Elad, and G. Sapiro, "Sparse representation for color image restoration," IEEE Trans. Image Process. **17**, 53–69 (2008).
20. R. Rubinstein, A. M. Bruckstein, and M. Elad, "Dictionaries for sparse representation modeling," Proc. IEEE **98**, 1045–1057 (2010).
21. L. Yuan, J. Sun, L. Quan, and H.-Y. Shum, "Progressive inter-scale and intra-scale non-blind image deconvolution," ACM Trans. Graph. **27**, 74 (2008).
22. J. Portilla, "Image restoration through l0 analysis-based sparse optimization in tight frames," in *Proceedings of the International Conference on Image Processing* (IEEE, 2009), pp. 3909–3912.
23. Z. Ming, Z. Wei, and W. g. Zhile, "Satellite image deconvolution based on nonlocal means," Appl. Opt. **49**, 6286–6294 (2010).
24. J. Ni, P. Turaga, V. M. Patel, and R. Chellappa, "Example-driven manifold priors for image deconvolution," IEEE Trans. Image Process. **20**, 3086–3096 (2011).
25. F. Xue, F. Luisier, and T. Blu, "Multi-Wiener SURE-LET deconvolution," IEEE Trans. Image Process. **22**, 1954–1968 (2013).
26. H. Yang, M. Zhu, Z. Zhang, and H. Huang, "Guided filter based edge-preserving image non-blind deconvolution," in *Proceedings of 20th IEEE International Conference on Image Processing* (IEEE, 2013).
27. P. Toft, "The Radon transform—theory and implementation," Ph.D. thesis (Technical University of Denmark, 1996).
28. K. He, J. Sun, and X. Tang, "Guided image filtering," in Proceedings of the 11th European Conference on Computer Vision: Part I, Heidelberg (2010), pp. 1–14.